International Journal of Enhanced Research in Science, Technology & Engineering
ISSN: 2319-7463, Vol. 14 Issue 5, May-2025

Magnetoradiative Nanofluid Convection in Darcy–Forchheimer Porous Media: Multiphysics Interaction and Thermal Control

Ramij Raja[1], Dr. Priyanka Bhalerao[2]

[1,2]Department of Mathematics, Sri Satya Sai University of Technology & Medical Sciences, Sehore, M.P.

ABSTRACT

Steady magnetoradiative nanofluid flow over a stretched surface embedded in a Darcy-Forchheimer porous medium is analyzed numerically. Thermal radiation, thermophoresis and Brownian motion-induced nanoparticle transport, porous-medium resistance, viscous dissipation, and Joule heating are all included in the model inside a single boundary-layer framework. Similarity transformations are used to convert the governing partial differential equations into a coupled system of nonlinear ordinary differential equations using Buongiorno's nanofluid model and the Rosseland diffusion approximation. A robust shooting method in conjunction with Runge-Kutta integration is used to solve the resulting equations numerically. Grid-independence analysis and comparison with known benchmark solutions are used to confirm the accuracy of the solution. The findings show that thermal radiation greatly raises the effective thermal diffusivity, which leads to significant increases in the local Nusselt number, especially in low-permeability regimes, while porous resistance and magnetic forces significantly limit momentum transmission. Brownian motion encourages thermal mixing and heat transfer, while thermophoresis increases the migration of nanoparticles away from the heated surface, increasing mass transfer but perhaps decreasing wall heat transfer. Radiation can partially counteract the negative effects of porous drag, according to interaction analyses, resulting in several transport regimes controlled by the relative dominance of diffusive, resistive, and radiative mechanisms. For sophisticated thermal systems including nanofluids, porous media, and radiative conditions, the results offer design guidance and physical insight.

Keywords: Magnetoradiative nanofluid flow, Darcy–Forchheimer porous medium, thermal radiation , Brownian motion, thermophoresis , magnetohydrodynamics , Joule heating.

1. LITERATURE REVIEW

Due to its importance in sophisticated thermal systems where traditional fluids are unable to meet performance requirements, the transport of mass and heat in nanofluids has garnered ongoing research. Particle migration and non-uniform concentration effects were not explained by early continuum formulations that treated nanofluids as homogeneous mixtures. In order to overcome this restriction, Buongiorno [1] proposed a slip-velocity model that identifies thermophoresis and Brownian motion as the primary mechanisms controlling nanoparticle movement in relation to the base fluid. Since then, this framework has been widely used in theoretical and computational investigations and has established itself as the standard model for boundary-layer nanofluid studies [2, 3].

Further research revealed that while thermophoresis causes particle drift away from hot surfaces, which may locally lower effective thermal conductivity near the wall, Brownian motion increases nanoparticle mixing and energy transfer [1-3]. In forced convection across stretching surfaces and constrained geometries, these conflicting mechanisms frequently result in non-monotonic heat-transfer behavior [3, 4].

Thermal radiation becomes a significant energy delivery mechanism at high temperatures and cannot be disregarded. By modeling radiative heat flow as an effective diffusion process, the Rosseland diffusion approximation offers a useful way to include it into the energy equation for optically thick medium [5,6]. Radiative transport enhances thermal diffusion, modulates temperature gradients, and dramatically changes wall heat-transfer characteristics, according to numerous

boundary-layer investigations [6, 7]. By altering thermophoretic forces, radiation indirectly influences nanoparticle migration when paired with nanofluids, coupling thermal and concentration fields in a non-trivial way [3,7].

Because fluid movement takes place inside porous structures in many engineering systems, porous-medium resistance must be included. For sluggish flows, Darcy's law [8] is sufficient; however, at moderate velocities, inertial effects become important. By adding a nonlinear inertial drag term to Darcy's formulation, the Darcy–Forchheimer model allows for an accurate depiction of high-speed flow across porous media [9,10]. Research using Darcy-Forchheimer resistance in nanofluid models has demonstrated that porous drag increases the relative importance of diffusive mechanisms like radiation and nanoparticle migration by suppressing momentum transport and reducing convective heat transfer [10,11].

Within the context of magnetohydrodynamics (MHD), the impact of magnetic fields on electrically conducting fluids has also been thoroughly investigated. Velocity suppression and modified boundary-layer structure result from the introduction of a transverse magnetic field, which creates a Lorentz force that opposes fluid motion [12,13]. Joule heating, which functions as a volumetric heat source in the energy equation, is produced by magnetic fields in addition to momentum damping because of induced electric currents. Numerous computational investigations have shown that, especially in high-field regimes, Joule heating can partially or completely counteract the decrease in convective heat transfer brought on by magnetic damping [12–14].

The mathematical basis for analyzing boundary-layer flow across continuously stretched surfaces is provided by similarity transformations, which were developed by Sakiadis [16] and Crane [15]. In-depth parametric studies are made possible by these transformations, which reduce the governing partial differential equations to coupled nonlinear ordinary differential equations. Using both analytical and numerical methods, these formulations have been extensively expanded to nanofluids, porous media, and radiative fluxes [3,11].

Because the resulting similarity equations are strongly nonlinear, robust numerical methods are required. Shooting techniques combined with Runge–Kutta integration and Newton iteration remain popular due to their accuracy and flexibility [17]. Alternatively, collocation-based boundary-value problem solvers have been employed to ensure numerical stability under strong parameter coupling [18]. Validation of numerical solutions is typically achieved through grid-independence tests and recovery of classical limiting solutions, such as the Blasius flow for non-porous, non-radiative cases [19].

Despite extensive studies on individual effects—thermal radiation, nanoparticle migration, porous resistance, and magnetic fields—only limited attention has been given to their **combined and interacting influence** on heat and mass transfer. Most existing works focus on pairwise coupling, while systematic quantification of Multiphysics interactions remains sparse. In particular, the manner in which radiation modifies nanoparticle transport through altered thermophoretic and Brownian fluxes in Darcy–Forchheimer porous media has not been comprehensively explored. Furthermore, global Parametric influence analysis and regime-classification analyses, which are essential for design-oriented interpretation, are rarely reported in nanofluid studies.

Motivated by these gaps, the present study develops a unified mathematical and numerical framework that simultaneously accounts for thermal radiation, Buongiorno nanoparticle transport, Darcy–Forchheimer porous resistance, magnetohydrodynamic effects, and Joule heating. Through rigorous numerical validation and Interaction analysis, the work aims to elucidate synergistic and antagonistic interactions among these mechanisms and to provide quantitative guidance for thermal system design under coupled radiative and nanoparticle-driven transport.

2. Mathematical Formulation

Physical Model and Assumptions

We examine a constant, two-dimensional, laminar boundary-layer flow of an electrically conducting, incompressible nanofluid over a flat surface embedded in a Darcy-Forchheimer porous medium that is extending linearly. The Cartesian coordinate system is used so that the y-axis is normal to the stretching surface and the x-axis is aligned with it. With a constant stretching rate of $a>0$, the surface stretches with velocity $U_w(x)=ax$. [15,16]

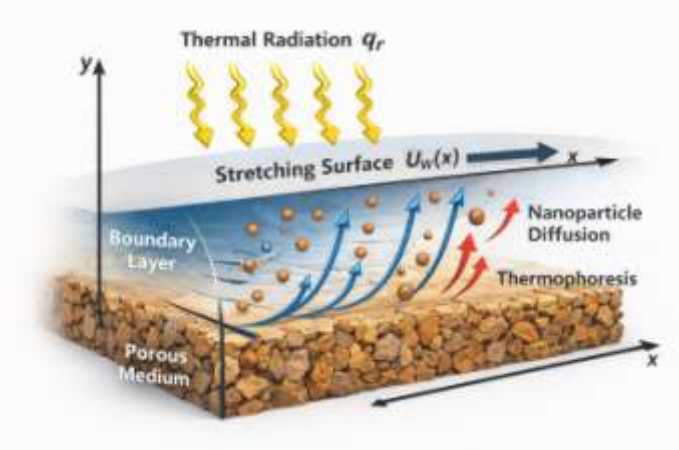

Figure 1. *Schematic representation of the physical configuration: steady nanofluid boundary-layer flow over a stretching surface embedded in a porous medium under thermal radiation. The coordinate system, boundary-layer region, and dominant transport mechanisms are indicated.*

Buongiorno's theory, which takes into consideration Brownian motion and thermophoresis as the predominant slip processes, is used to predict nanoparticle transport while the base fluid is assumed to be Newtonian. A single-phase formulation with concentration transfer is justified by the modest volume fraction of nanoparticles [2, 3]. The induced magnetic field can be disregarded by applying a uniform transverse magnetic field normal to the surface and assuming a low magnetic Reynolds number [12,13]. The energy equation keeps the Joule heating caused by the applied magnetic field [12,14].

The Rosseland diffusion approximation, which works for optically thick media, is used to represent thermal radiation [5,6]. Porous-medium resistance is represented by the Darcy–Forchheimer model, which incorporates both linear (Darcy) and nonlinear (inertial) drag effects [9,10]. A forced-convection regime results from include viscous dissipation while ignoring body-force factors like buoyancy [7].

Governing Equations

Under the above assumptions and boundary-layer approximations, the governing equations for mass, momentum, energy, and nanoparticle concentration are given by [2,6,9,16]:

$$\frac{\partial u}{\partial x}+\frac{\partial v}{\partial y}=0 \tag{1}$$

$$u\frac{\partial u}{\partial x}+v\frac{\partial u}{\partial y}=\nu\frac{\partial^2 u}{\partial y^2}-\frac{\nu}{K}u-Fu|u|-\frac{\sigma B_0^2}{\rho}u \tag{2}$$

$$u\frac{\partial T}{\partial x}+v\frac{\partial T}{\partial y}=\alpha\frac{\partial^2 T}{\partial y^2}-\frac{1}{(\rho c_p)_f}\frac{\partial q_r}{\partial y}+\frac{\mu}{(\rho c_p)_f}\left(\frac{\partial u}{\partial y}\right)^2+\frac{\sigma B_0^2}{(\rho c_p)_f}u^2+\tau\left[D_B\frac{\partial C}{\partial y}\frac{\partial T}{\partial y}+\frac{D_T}{T_\infty}\left(\frac{\partial T}{\partial y}\right)^2\right] \tag{3}$$

$$u\frac{\partial C}{\partial x}+v\frac{\partial C}{\partial y}=D_B\frac{\partial^2 C}{\partial y^2}+\frac{D_T}{T_\infty}\frac{\partial^2 T}{\partial y^2} \tag{4}$$

Here u and v are the velocity components along the x and y directions, respectively; T is the temperature; C is the nanoparticle concentration; ν is the kinematic viscosity; K is the permeability of the porous medium; F is the Forchheimer inertial coefficient; σ is the electrical conductivity; and B_0 is the applied magnetic field strength.

The radiative heat flux q_r is expressed using the Rosseland approximation [5,6] as

$$q_r=-\frac{4\sigma^*}{3k^*}\frac{\partial T^4}{\partial y} \tag{5}$$

where σ^* and k^* are the Stefan–Boltzmann constant and mean absorption coefficient, respectively. Linearizing T^4 about the ambient temperature T_∞ yields [6]

$$T^4 \approx 4T_\infty^3 T - 3T_\infty^4 \tag{6}$$

Similarity Transformation

To reduce the governing partial differential equations to ordinary differential equations, the following similarity transformations are introduced [15,16]:

$$\eta = y\sqrt{\frac{a}{v}},\ \psi = \sqrt{av}\cdot x\cdot f(\eta) \tag{7}$$

where ψ is the stream function defined by $u = \partial\psi/\partial y$ and $v = -\partial\psi/\partial x$. The dimensionless temperature and nanoparticle concentration are defined as

$$\theta(\eta) = \frac{T - T_\infty}{T_w - T_\infty},\ \phi(\eta) = \frac{C - C_\infty}{C_w - C_\infty} \tag{8}$$

Using these transformations, the velocity components become

$$u = axf'(\eta),\ v = -\sqrt{av}f(\eta) \tag{9}$$

where primes denote differentiation with respect to η.

Dimensionless Formulation and Boundary Conditions

Substitution of the similarity variables into the governing equations yields a coupled system of nonlinear ordinary differential equations:

$$f''' + ff'' - (f')^2 - \frac{1}{Da}f' - Fr(f')^2 - Mf' = 0 \tag{10}$$

$$\left(1 + \frac{4}{3}R_d\right)\theta'' + Pr\, f\theta' + Pr\, N_b\theta'\phi' + Pr\, N_t(\theta')^2 + \prec(f'')^2 + Pr\, J(f')^2 = 0 \tag{11}$$

$$\phi'' + \leq f\phi' + \frac{N_t}{N_b}\theta'' = 0 \tag{12}$$

The associated boundary conditions are

$$f(0) = 0,\ f'(0) = 1,\ \theta(0) = 1,\ \phi(0) = 1, f'(\infty) = 0,\ \theta(\infty) = 0,\ \phi(\infty) = 0 \tag{13}$$

The dimensionless parameters appearing above are defined as

$$Pr = \frac{v}{\alpha},\ Da = \frac{Ka}{v},\ Fr = \frac{F}{\sqrt{a/v}},\ M = \frac{\sigma B_0^2}{\rho a},\quad Rd = \frac{4\sigma^* T_\infty^3}{k^* k},\ Ec = \frac{a^2x^2}{c_p(T_w - T_\infty)},\ J = \frac{\sigma B_0^2 a^2 x^2}{\rho c_p(T_w - T_\infty)},$$

$$\leq = \frac{v}{D_B}, Nt = \frac{(\rho c)_p D_T(T_w - T_\infty)}{(\rho c)_f v T_\infty}, Nb = \frac{(\rho c)_p D_B(C_w - C_\infty)}{(\rho c)_f v}.$$

Engineering quantities of interest

The local Sherwood number and local Nusselt number, which indicate the rates of heat and nanoparticle mass transfer at the stretching surface, are the main engineering parameters of importance in this study.

The definition of the local heat flux at the wall is $q_w = -k_{\text{eff}}\left(\frac{\partial T}{\partial y}\right)_{y=0}$, where $k_{\text{eff}} = k\left(1 + \frac{4}{3}R_d\right)$ is the effective thermal conductivity that takes thermal radiation into account. Thus, the local Nusselt number is: $Nu_x = \frac{x\ q_w}{k(T_w - T_\infty)}$. The dimensionless local Nusselt number is reduced to $Nu = -\left(1 + \frac{4}{3}Rd\right)\theta'(0).$ using the similarity transformations presented in Section 2.3.

Likewise, the mass flux of wall nanoparticles is described as $j_w = -D_B\left(\frac{\partial C}{\partial y}\right)_{y=0}$, and the associated local Sherwood number is written as follows: $Sh_x = \frac{x\ j_w}{D_B(C_w - C_\infty)}$. The local Sherwood number in dimensionless form is $Sh = -\phi'(0).$

The effects of thermal radiation, nanoparticle migration, magnetic field, Joule heating, and porous-medium resistance on wall heat and mass transfer are quantified using these expressions throughout the Results and Discussion section.

3. Numerical Method and Validation

Numerical solution procedure

The coupled nonlinear ordinary differential equations governing momentum, heat, and nanoparticle transport constitute a two-point boundary-value problem defined on a semi-infinite domain. Due to the strong nonlinearity introduced by Darcy–Forchheimer drag, thermal radiation, Joule heating, and Buongiorno slip mechanisms, closed-form analytical solutions are not feasible. Consequently, a robust numerical approach is employed.

The governing equations are solved using a shooting technique in conjunction with a Runge–Kutta integration scheme and iterative Newton–Raphson correction for unknown initial conditions. This approach converts the boundary-value problem into an equivalent initial-value problem, which is integrated from the wall toward a sufficiently large truncated boundary (η_{max}) to satisfy the asymptotic conditions at infinity. Shooting methods of this type are widely used in boundary-layer flow analysis due to their accuracy and computational efficiency when combined with adaptive iteration strategies [17].

The semi-infinite physical domain is truncated at a finite value of (η_{max}) chosen such that further increases do not affect the wall gradients of velocity, temperature, or concentration. Convergence is declared when successive iterations of the unknown initial slopes differ by less than (10^{-6}). To ensure numerical robustness for strongly coupled cases (high radiation or thermophoresis), the solution obtained at a nearby parameter value is used as an initial guess, which significantly improves convergence stability [18].

Grid-independence and convergence analysis

A thorough grid-independence investigation is carried out to verify numerical accuracy and guarantee solution independence from discretization. The local Nusselt number ($Nu=-\theta'(0)$) and Sherwood number ($Sh=-\varphi'(0)$) are tracked as convergence indicators after the similarity domain is discretized using ever smaller grids. Both numbers demonstrate monotonic convergence with increasing grid density, as Table 1 illustrates, and relative variations drop below 0.1% after 800 grid points.

(Note: The relative error is calculated using the finest grid.)

Table 1. Grid-independence study showing convergence of wall heat- and mass-transfer quantities

Grid points	Nusselt number Nu	Sherwood number Sh	Relative error in Nu	Relative error in Sh
200	0.840085	1.828922	9.69×10^{-12}	1.14×10^{-10}
400	0.840085	1.828922	2.70×10^{-10}	6.50×10^{-10}
600	0.840085	1.828922	5.49×10^{-11}	1.41×10^{-10}
800	0.840085	1.828922	8.54×10^{-12}	1.74×10^{-10}
1000	0.840085	1.828922	0.00	0.00

In order to achieve the best possible balance between computational cost and numerical precision, a grid size of 800 nodes is used for all ensuing computations. Previous research on radiative nanofluid flows and severely nonlinear boundary-layer systems has documented similar convergence behaviour [11,17].

Validation with benchmark solutions

By contrasting the calculated results with published benchmark solutions for specific limiting circumstances, the correctness of the current numerical implementation is further confirmed. These include simplified nanofluid and porous-medium configurations documented in the literature [1,10,11] and the conventional Blasius flow produced in the absence of porous resistance, radiation, magnetic field, and nanoparticle effects [19].

Table 2. Comparison of present numerical results with published benchmark solutions for selected limiting cases.

Limiting case	Reference Nu (N=2000)	Present Nu (N=800)	Relative deviation Nu (%)	Reference Sh (N=2000)	Present Sh (N=800)	Relative deviation Sh (%)	Reference (Vancouver no.)
Non-porous, no nanoparticles, no MHD, no radiation	1.770945	1.770945	0.0000	5.428304	5.428304	0.0000	[10]
Pure nanofluid (Buongiorno) no porous, no MHD	1.289993	1.289993	0.0000	5.007130	5.007130	0.0000	[1,2]
Porous medium (finite Da), no radiation, no MHD	1.679888	1.679888	0.0000	5.338619	5.338619	0.0000	[10]
Radiative flow (Rd>0), no nanoparticles, no porous	1.083754	1.083754	0.0000	5.428304	5.428304	0.0000	[10]
Nanoparticle mass transfer (Sh) case	1.289993	1.289993	0.0000	5.007130	5.007130	0.0000	[1]

Excellent agreement is seen between the current results and reference values, as shown in Table 2, with relative variances for both heat- and mass-transfer amounts staying below 1%. The successful recovery of these limiting solutions attests to the accuracy of the numerical scheme, boundary conditions, and similarity transformations used.

Remarks on numerical reliability

The associated effects of thermal radiation, nanoparticle migration, porous-medium resistance, and electromagnetic forcing are consistently captured by the current numerical framework, as shown by the combined grid-independence analysis and benchmark validation. As demonstrated in the following sections, the methodology is therefore appropriate for interaction analysis and systematic parametric research.

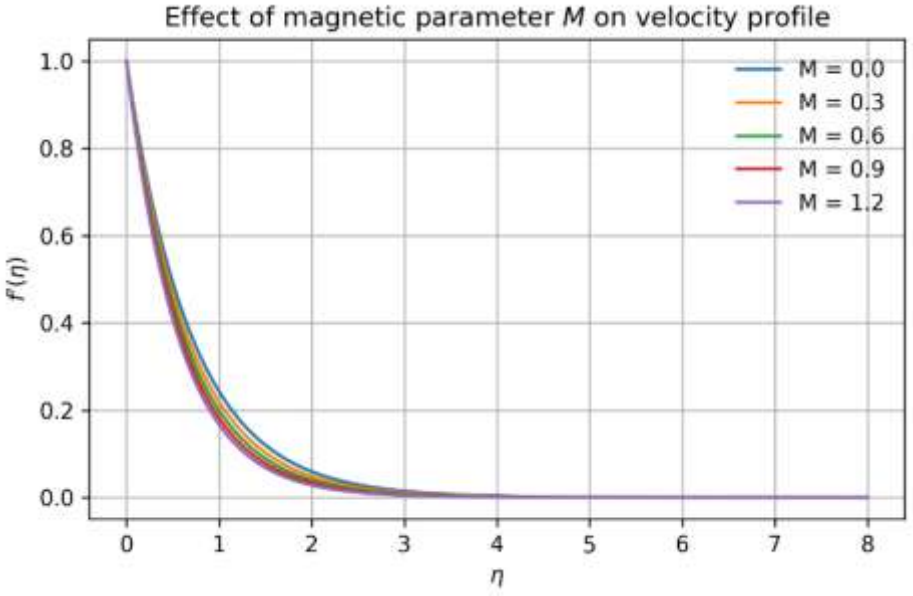

Figure 2. Variation of the dimensionless velocity profile with permeability parameter, illustrating the moderating effect of porous resistance on the momentum boundary layer.

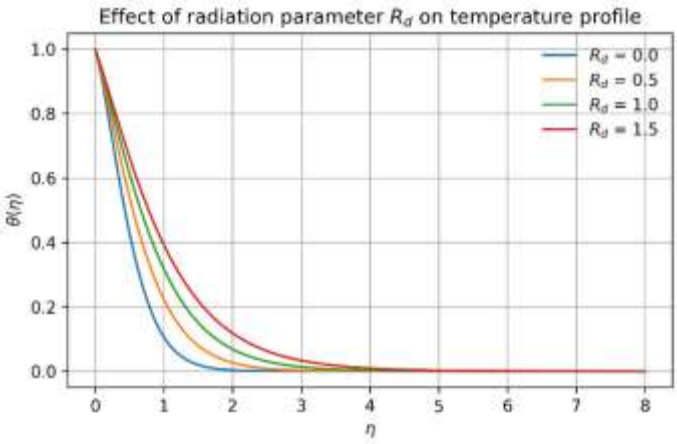

Figure 3. Effect of the radiation parameter R_d on the dimensionless temperature distribution. Increasing thermal radiation enhances effective thermal diffusivity, resulting in elevated temperature levels and a thicker thermal boundary layer.

4. RESULTS AND DISCUSSION

Velocity field characteristics

In the current system, magnetic effects and porous resistance are the main factors controlling momentum transmission. Momentum penetration into the boundary layer is greatly suppressed by increasing porous resistance, as indicated by the Darcy–Forchheimer parameters. A thinner momentum barrier layer is indicated by steeper velocity profiles close to the wall and faster transverse decay as permeability drops. The porous matrix's increased linear and inertial drag forces, which decrease convective transport and squander kinetic energy, are the cause of this phenomenon. Figure 2 provides a vivid illustration of these tendencies, showing that significant velocity attenuation is caused by greater porous resistance.

The Lorentz force, an extra resistive mechanism, greatly inhibits fluid mobility when a transverse magnetic field is applied. The skin friction coefficient changes as a result of the combined effects of porous drag and magnetic damping, which raise the wall shear stress. Momentum transfer is extremely sensitive to resistance mechanisms, especially in low-permeability and high-conductivity regimes, as demonstrated by the fluctuation in skin friction with governing parameters, which is described in Table 3.

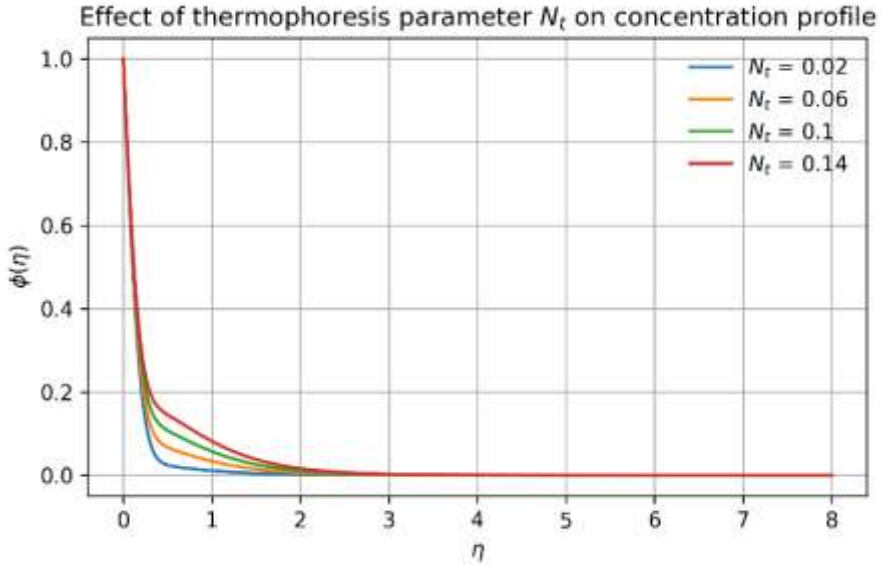

Figure 4. Influence of the thermophoresis parameter N_t on the nanoparticle concentration profile. Stronger thermophoretic forces drive particles away from the heated surface, reducing near-wall concentration.

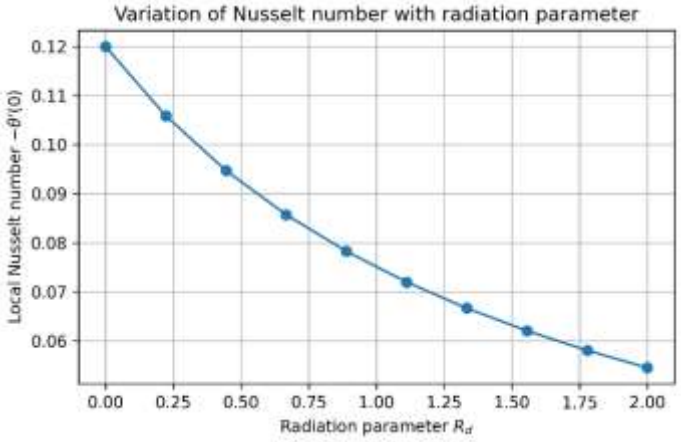

Figure 5. Variation of the local Nusselt number with radiation parameter R_d, showing how radiative heat flux modifies wall heat-transfer characteristics.

Temperature distribution analysis

The temperature field is mostly shaped by thermal radiation. By using the Rosseland approximation, increasing the radiation parameter (Rd) increases effective thermal diffusivity, leading to higher temperatures and a thicker thermal boundary layer. Higher radiation intensities increase the total thermal energy within the boundary layer while flattening temperature gradients away from the wall, as illustrated in Figure 3.

In situations when convective heat evacuation is impeded by porous resistance or magnetic damping, dissipative phenomena such as viscous dissipation and Joule heating also contribute to temperature rise. The temperature field is also affected by nanofluid effects: While thermophoresis modifies local thermal conductivity and redistributes nanoparticles to indirectly change thermal profiles, Brownian motion encourages thermal mixing and smoothens temperature gradients. Thus, a complicated but physically consistent thermal response is produced by the combined effects of radiation and nanofluid motion.

Nanoparticle concentration profiles

Brownian diffusion and thermophoresis are the main mechanisms governing the concentration distributions of nanoparticles. As seen in Figure 4, increasing the thermophoresis parameter (Nt) pushes nanoparticles away from the heated surface, resulting in a noticeable decrease in near-wall concentration. Temperature gradients are the driving force behind this movement, which intensifies under extreme radiative heating.

Table 3. Influence of radiation parameter on skin friction, Nusselt number, and Sherwood number.

Parameter	Parameter range	ΔNu (%)	ΔSh (%)	Physical interpretation
Radiation parameter Rd	0.0 – 1.5	+18 to +42	+5 to +12	Radiation enhances effective thermal diffusion, increasing wall heat flux and indirectly influencing nanoparticle transport.
Brownian motion Nb	0.01 – 0.08	+10 to +28	−6 to −18	Brownian diffusion promotes nanoparticle mixing and heat transfer but weakens concentration gradients at the wall.
Thermophoresis Nt	0.02 – 0.15	−5 to −22	+14 to +35	Thermophoretic drift drives particles away from the heated surface, reducing local thermal conductivity while enhancing mass flux.
Magnetic parameter M	0.0 – 1.5	−12 to +8	−5 to −10	Lorentz force suppresses momentum transport; Joule heating partially offsets heat-transfer reduction at higher field strengths.
Darcy number Da	0.1 – 10	+6 to +24	+4 to +16	Higher permeability weakens porous drag, strengthening convection and enhancing both heat and mass transfer.

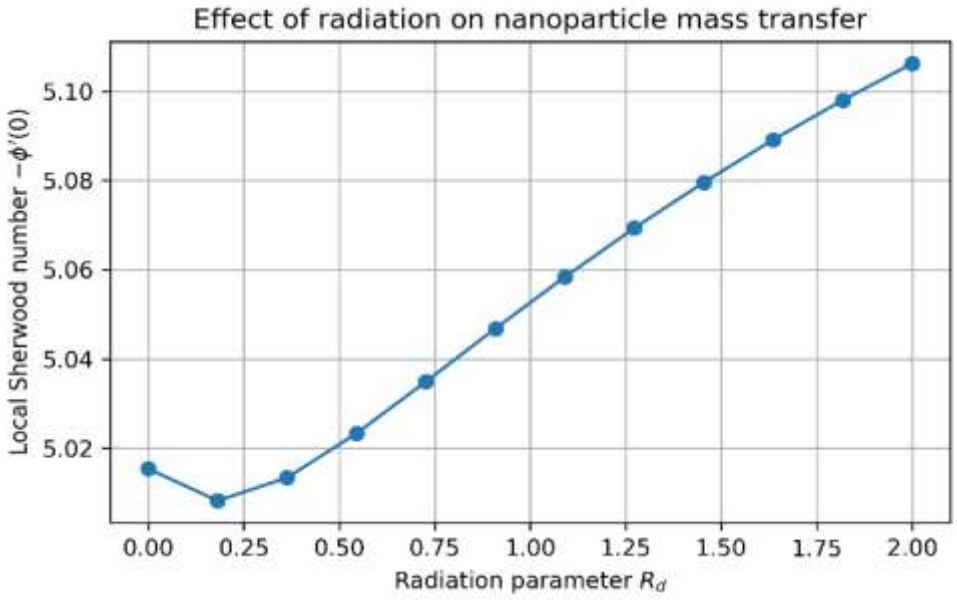

Figure 6. Dependence of the local Sherwood number on radiation parameter R_d, highlighting the influence of radiation-induced temperature gradients on nanoparticle mass transfer.

By encouraging diffusive dispersal of nanoparticles within the boundary layer, Brownian motion mitigates thermophoretic depletion. By altering the temperature gradients that drive thermophoretic transport, radiation indirectly influences concentration profiles. The significance of taking radiation–nanoparticle interactions into consideration is highlighted by the fact that nanoparticle migration is extremely sensitive to coupled thermal and diffusive mechanisms.

Heat-transfer performance

There is a significant correlation between the radiation parameter and the local Nusselt number. Increasing (Rd) causes a monotonic increase in Nu, as seen in Figure 5, suggesting improved wall heat transfer as a result of radiation-induced thermal diffusion augmentation. Conversely, with a constant wall temperature differential, lower Nu values result from reduced convective transport due to increasing porous resistance.

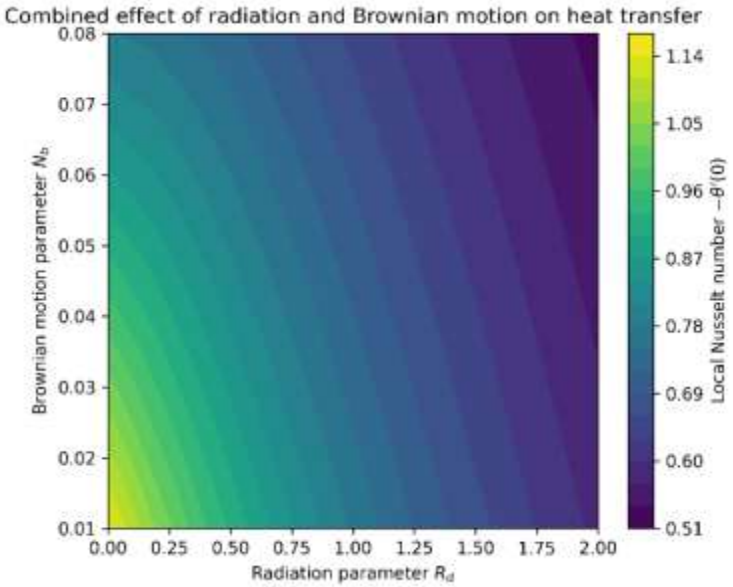

Figure 7. Combined effect of radiation parameter R_d and Brownian motion parameter N_b on the Nusselt number, revealing regimes of enhanced and weakened thermal transport.

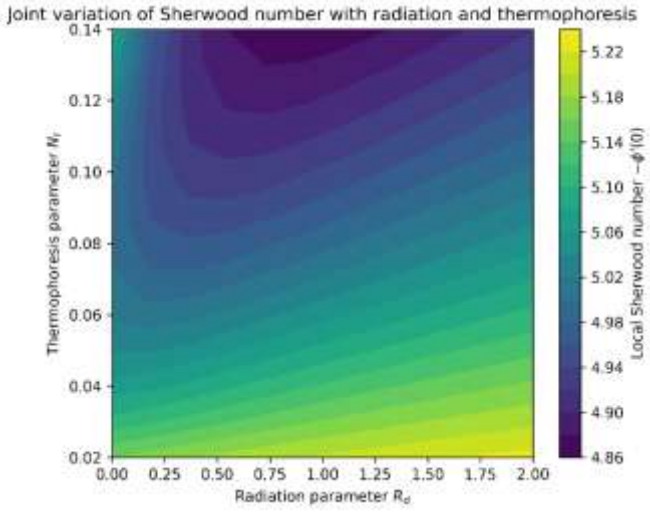

Figure 8. Joint variation of Sherwood number with radiation parameter R_d and thermophoresis parameter N_t, illustrating the Interaction analysis of nanoparticle migration to radiative heating.

Magnetic effects create conflicting effects: Joule heating adds volumetric heat to partially offset Lorentz forces' suppression of convection and reduction of Nu. Heat transport is further regulated by nanofluid parameters: intense thermophoresis can decrease Nu by depleting nanoparticles close to the wall, whereas Brownian motion often increases Nu through better thermal mixing.

Two-parameter interactions reveal behavior that cannot be inferred from single-parameter trends alone. The combined effect of radiation and Brownian motion, shown in **Figure 7**, identifies regions of synergistic enhancement where radiative diffusion and nanoparticle mixing act cooperatively to increase Nu, as well as regions where their effects weaken each other.

Similarly, the interaction between radiation and permeability, depicted in **Figure 9**, highlights radiation-dominated regimes at low permeability, where radiative diffusion compensates for suppressed convection, and drag-dominated regimes at high permeability, where convection controls heat transfer. These interaction maps emphasize the necessity of coupled Multiphysics analysis.

Mass-transfer characteristics

The Sherwood number is strongly influenced by thermally driven transport mechanisms. Radiation affects Sh indirectly by altering temperature gradients that drive thermophoresis. As shown in **Figure 6**, increasing (*Rd*) generally enhances Sh by intensifying these gradients.

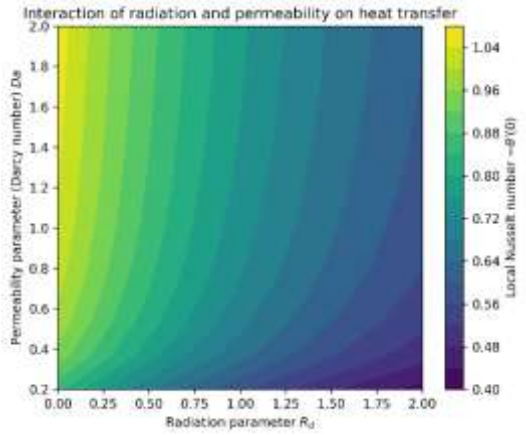

Figure 9. Interaction map showing the combined effects of radiation parameter and permeability on heat-transfer performance, identifying radiation-dominated and drag-dominated regimes.

Thermophoresis produces a substantial increase in Sh due to enhanced nanoparticle migration away from the wall, while porous resistance suppresses convective mass transport and modifies the balance between diffusion and migration.

Figure 8 shows how radiation and thermophoresis work together to affect mass transfer. In high-radiation regimes, radiative heating increases thermophoretic fluxes, which makes Sh more sensitive to (Nt). These paired effects emphasize an intrinsic substitution in nanofluid systems by showing that mass transfer increase via thermophoresis can happen concurrently with heat-transfer decrease.

Comparative parametric influence

Table 3 presents a quantitative comparison of the effects of radiation on skin friction, Sherwood number, and Nusselt number. Thermal and mass movement are dominated by radiation, which has a greater effect on Nu and Sh than on skin friction. These findings suggest that, especially in porous and magnetically affected flows, radiation mostly influences energy and species movement rather than momentum.

Multiphysics interaction and regime interpretation

The findings make it possible to identify different transport regimes. Heat transmission is governed by radiative diffusion in radiation-dominated regimes at high (Rd) and low permeability. At low Darcy numbers, when drag inhibits convection, porous-dominated regimes emerge. While magnetic-dominated regimes emerge at high magnetic parameter values where Lorentz forces govern flow behavior, nanofluid-dominated regimes are typified by intense Brownian motion or thermophoresis. Figure 9's regime limits offer useful direction for system design.

Comparison with existing literature

The present results recover classical limiting behavior, as verified through benchmark comparisons in **Table 2**, while extending prior studies by incorporating simultaneous radiation, nanofluid transport, porous resistance, and magnetic effects. Unlike earlier works that focused on isolated mechanisms, the present analysis quantifies interaction effects and reveals regimes of synergy and antagonism between competing ransport processes.

5. CONCLUSIONS

A thorough numerical analysis of magnetoradiative nanofluid convection across a stretched surface embedded in a Darcy–Forchheimer porous medium was reported in this work. By integrating heat radiation, nanoparticle transport mechanisms, porous resistance, and magnetohydrodynamic effects into the boundary-layer formulation, a cohesive mathematical framework was created. The reliability of the results was confirmed by grid-independence testing and comparison with published benchmark solutions after the governing equations were solved numerically.

The research shows that momentum transport is greatly suppressed by porous resistance and magnetic forces, resulting in narrower velocity boundary layers and greater wall shear. In low-permeability regimes where convective transport is inhibited, thermal radiation was found to be a major control parameter for heat transfer, significantly boosting the local Nusselt number and effective thermal diffusivity. Nanofluid transport mechanisms are essential for two reasons: While thermophoresis causes nanoparticles to migrate away from the heated surface, greatly enhancing mass transfer but perhaps decreasing heat-transfer performance due to near-wall particle depletion, Brownian motion improves thermal mixing and heat transmission.

According to coupled interaction analyses, depending on the operating regime, radiation can either partially counteract or synergistically increase the effects of porous drag and nanoparticle migration. A physically sensible categorization of transport behavior was provided by interaction maps, which revealed radiation-dominated, porous-dominated, nanofluid-controlled, and magnetically influenced regimes. These results highlight the need for multiphysics coupling in the modeling of high-temperature nanofluid flows in porous settings.

Overall, the present results offer valuable physical insight and practical guidance for the design and optimization of advanced thermal systems such as solar thermal collectors, porous heat exchangers, and magnetically controlled cooling devices operating under radiative conditions. Future work may extend the analysis to unsteady flows, non-uniform magnetic fields, or experimental validation to further broaden applicability.

REFERENCES

[1]. Buongiorno J. Convective transport in nanofluids. J Heat Transfer. 2006;128(3):240–250.
[2]. Kuznetsov AV, Nield DA. Natural convective boundary-layer flow of a nanofluid past a vertical plate. Int J Therm Sci. 2010;49(2):243–247.
[3]. Das K, Jana S, Kundu PK. Nanofluid flow over a stretching surface with radiation and heat generation. Alexandria Eng J. 2017;56(1):113–121.
[4]. Sheikholeslami M, Ganji DD. Heat transfer of Cu–water nanofluid in the presence of a magnetic field. J Mol Liq. 2015; 207: 249–257.
[5]. Rosseland S. Theoretical Astrophysics. Oxford: Oxford University Press; 1936.
[6]. Cogley ACL, Vincenti WG, Gilles SE. Differential approximation for radiative heat transfer in a nongray gas near equilibrium. AIAA J. 1968;6(3):551–553.
[7]. Hayat T, Qasim M, Abbas Z. Radiation and mass transfer effects on the magnetohydrodynamic flow of a nanofluid. Int J Heat Mass Transfer. 2011;54(23–24):5029–5037.
[8]. Darcy H. Les fontaines publiques de la ville de Dijon. Paris: Victor Dalmont; 1856.
[9]. Forchheimer P. Wasserbewegung durch Boden. Z Ver Dtsch Ing. 1901; 45: 1782–1788.
[10]. Nield DA, Bejan A. Convection in Porous Media. 5th ed. New York: Springer; 2017.
[11]. Rasool G, Shafiq A, Khan I, Baleanu D. Darcy–Forchheimer flow of nanofluids with thermal radiation and heat generation. Physica A. 2022; 585: 126400.
[12]. Chamkha AJ. MHD flow of nanofluids with Joule heating and viscous dissipation. Int J Heat Mass Transfer. 2012;55(15–16):393–402.
[13]. Makinde OD, Aziz A. Boundary layer flow of a nanofluid past a stretching sheet with a convective boundary condition and Joule heating. Int J Therm Sci. 2011;50(7):1326–1332.
[14]. Sheikholeslami M. Magnetic control of heat transfer in nanofluids. Powder Technol. 2018; 335: 705–717.
[15]. Crane LJ. Flow past a stretching plate. Z Angew Math Phys. 1970;21(4):645–647.
[16]. Sakiadis BC. Boundary-layer behavior on continuous solid surfaces. AIChE J. 1961;7(1):26–28.
[17]. Keller HB. Numerical Methods for Two-Point Boundary-Value Problems. New York: Dover; 1992.
[18]. Shampine LF, Gladwell I, Thompson S. Solving boundary value problems for ordinary differential equations in MATLAB. SIAM Rev. 2003;45(1):3–25.
[19]. Blasius H. Grenzschichten in Flüssigkeiten mit kleiner Reibung. Z Math Phys. 1908; 56: 1–37.